Nano Energy 77 (2020) 105171

Contents lists available at ScienceDirect

Nano Energy

journal homepage: http://www.elsevier.com/locate/nanoen

Soft robots with self-powered configurational sensing

Jian Chen [a,b,1], Kai Han [a,b,1], Jianjun Luo [a,b], Liang Xu [a,b], Wei Tang [a,b,**], Zhong Lin Wang [a,b,c,*]

[a] CAS Center for Excellence in Nanoscience, Beijing Key Laboratory of MicroNano Energy and Sensor, Beijing Institute of Nanoenergy and Nanosystems, Chinese Academy of Sciences, Beijing, 100083, China

[b] School of Nanoscience and Technology, University of Chinese Academy of Sciences, Beijing, 100049, China

[c] School of Materials Science and Engineering, Georgia Institute of Technology, Atlanta, GA, 30332-0245, USA

ARTICLE INFO

Keywords:
Triboelectric nanogenerator
Soft robots
Self-powered sensor
Proprioception

ABSTRACT

In recent years, soft robots have been evolved at a rapid pace. Soft robots possess infinite degrees of freedom because of the stretchability, which also poses a great challenge for sensing and controlling. Triboelectric nanogenerator (TENG) holds a promising potential as a self-powered sensor for soft robots due to its high sensitivity, flexibility and simplicity. In this work, a sensorized pneumatic soft actuator (PSA) is designed by integrating TENG based self-powered sensors inside the chambers. The sensors give feedback on the dynamic and static configurations of the PSA. The output voltage of a TENG has a good linear relationship with the local bending angle. In addition, the voltage output of all TENGs connected in parallel is linearly related to the total bending angle of the PSA. Applications of the sensorized PSA in a universal soft gripper and humanoid fingers are demonstrated. The self-powered sensors can give corresponding feedback when the soft gripper catches cups with different sizes/weights or when the humanoid fingers make different gestures. The sensorized PSA pave the way for precise control and safely interaction.

1. Introduction

Inspired by worms and elephant trunks, soft robots have aroused great interest and been developing at a rapid pace [1–3]. A soft robot that usually made of silicone rubber has advantages of soft, lightweight, multi-degree of freedom, etc. [4,5] Soft robots are adaptable to a broad range of tasks by passively changing its shape and locomotion. Therefore, soft robots have a great potential to revolutionize the humanoid robots and the human-machine interaction [6,7].

Compared to their rigid-body counterparts, the emerging soft robots possess infinitely passive degrees of freedom as a result of continuously deformable silicone bodies. These emphasize the needs for completely different sensing approaches, as well as modeling and controlling [8–12]. Several sensing schemes have been developed for soft robots perceiving, such as resistance strain sensor [13,14], Hall effect bending sensor [15] and optical fiber strain sensor [16]. However, there are still many challenges in the aspects of cost, energy consumption, space resolution and sensitivity, materials and process compatibility.

Triboelectric nanogenerator, based on the coupling effect of contact electrification and electrostatic induction, can actively respond to different types of mechanical triggers and show advantages of light weight, low cost, vast materials choice (rigid and soft) and high response [17–22]. TENG has been widely used as self-powered sensors for pressure, touch, movement and gesture [23–26], which are also suitable for soft robots [27–29]. Although several literatures have applied TENGs into soft robots, they mainly focus on exteroceptive functions such as touch and pressure sensing for human interaction [30–35].

Here, TENGs are integrated into a PSA as proprioception sensors of configuration. A piece of conductive sponge sheet is placed in each chamber of the PSA to form a single electrode TENG. The expansion/contraction of a chamber causes the PSA bending at nearby, as well as the contact/separation of the TENG. The voltage of the TENG is linearly related to the expansion degrees of the chamber and the local bending angle. Connected in parallel, the self-generated output voltage of all TENGs is linearly related to the total bending angle of the PSA. As demonstrations, the sensorized PSA could be assembled into a universal

* Corresponding author. CAS Center for Excellence in Nanoscience, Beijing Key Laboratory of MicroNano Energy and Sensor, Beijing Institute of Nanoenergy and Nanosystems, Chinese Academy of Sciences, Beijing 100083, China.,

** Corresponding author. CAS Center for Excellence in Nanoscience, Beijing Key Laboratory of MicroNano Energy and Sensor, Beijing Institute of Nanoenergy and Nanosystems, Chinese Academy of Sciences, Beijing 100083, China.

E-mail addresses: tangwei@binn.cas.cn (W. Tang), zhong.wang@mse.gatech.edu (Z.L. Wang).

[1] These authors contributed equally to this work.

https://doi.org/10.1016/j.nanoen.2020.105171
Received 13 May 2020; Received in revised form 23 June 2020; Accepted 2 July 2020
Available online 25 July 2020

soft gripper and humanoid fingers. When the gripper picks up cups, the voltage of the TENG is related to their sizes and weights. The humanoid fingers could make gestures and give signal feedback. The self-powered TENG sensors endow the PSA with proprioception function, which make it more controllable and safer when it interacts with environments or humankind.

2. Results and discussion

Fig. 1a illustrates the fabrication process of the sensorized PSA, which is mainly composed of a series of molding and demolding processes. Compared to the ordinary PSA, the sensorized PSA needs only one extra step, placing electrodes inside the chambers, as labeled 3 in Fig. 1a. One end of the electrode is fixed on the bottom layer during curing process to keep erecting in the chamber's center. Based on previous research, the conductive sponge is selected because it can be fixed well to silicone rubber by nest with each other. And the porous structure of the sponge does not influence the pneumatic process because it is air permeable [36]. The sponge electrode is very light and the weight of all 10 electrodes was only 0.2 g, which did not add burden to the PSA. Fig. 1b shows the sensorized PSAs under original flat state and pressured bending state. The PSA are assembled into a universal gripper that able to manipulate objects with different sizes or weights (Fig. 1c), where gesture sensing is very importance for controlling. Furthermore, the sensorized PSA can be wear on hands for assisting (Fig. 1d).

Since traditional rigid sensors is not suitable for a soft and stretchable PSA body, it is urgent to develop new sensing technology. The most common sensing scheme is by embedding strain sensors inside the inextensible bottom layer, like optical fiber and resistance wire. The bending radius of the PSA can be derived from the strain signal based on the rough approximate that the curvature of the fiber/wire is a constant. Here, a new solution is provided. TENGs are placed inside the chambers instead of the bottom layer to detect the expansion of the chamber and the bending angle of the PSA, as shown in Fig. 2a. The working principle of the TENG is illustrated in Fig. 2b. The inner wall of the chamber and the sponge electrode together form a single-electrode TENG. According to the triboelectric series, the silicone chamber is more electro-negative than the sponge electrode (Nickle). In the contacted state, the silicone rubber will get electrons from the electrode while the electrode contains equal positive charge. At the inflation state, the PSA is driven to bend by pressured air. The negatively charged silicone chamber expands and generally separates from the electrode. The positive charge flows out of the electrode to balance the potential rising. At the deflation state, the chamber slowly contracts back to its original shape. And the charged silicone contacts with the electrode again. The positive charge flow into the electrode due to the electrostatic induction. The electrostatic potential distribution was simulated by a Finite Element Software and is shown in Fig. 2c. The total charges on the silicone rubber surface was set to −2 nC, based on the measured transferred charges. The potential distribution of the contacted state is shown in the left of Fig. 2c, with the maximum potential of about −41 V. In the separated state, the potential distribution of the chamber is shown in the right with the maximum potential of about −35 V. Therefore, the potential difference of a chamber between contacted and separated state is approximately 6 V.

A test system was established to investigate the performance of the sensorized PSA, as illustrated in Fig. 2d. A syringe (60 mL, 90 mm) driven by a linear motor was utilized to provide the pneumatic source of the PSA, which is very convenient to control the parameters such as the gas volume and flow rate. Electrical outputs such as open circuit voltage, short circuit current, and transferred charges were measured by a electrometer (Keithley 6514). The pressure inside the chamber was recorded by the air gauge and the shape of the PSA was recorded by a digital camera simultaneously. The open circuit voltage of a single TENG is shown in Fig. 2e. The peak voltage was about 5.7 V, which is approximate to the simulation result. The amount of transferred charges was about 2.5 nC (Fig. 2f). To test the stability of the sensorized PSA, the linear motor was set at reciprocation motion to provide periodic pneumatic pressure for the PSA. After continuously working for 3 h (~7500 cycles), the output voltage of the TENG was stable at about 5.5 V without obvious attenuation (Fig. 2g). It indicates that both the PSA and TENG have good stability. Furthermore, the influence of the humidity or water was investigated. At first, the dry PSA was suspended in the air for testing. The open circuit voltage of the TENG was about 3 V. Then the PSA was completely submerged into water. The voltage increased to approximately 15 V, which is nearly 5 times higher than that in air. Then, the PSA was pulled out of water and hanged in the air. The external surface of the PSA was still wet, but the output voltage dropped to about 3 V immediately, as same as the completely dry state (Fig. 2h). The corresponding transferred charges is shown in Fig. 2i. The transferred charges of both the dry state and wet state were about 1 nC. While under water, the transferred charges increased to 4.5 nC. The TENG output had no different between dry and wet PSA, indicating that humidity does not affect the TENG performance. This is because the PSA was well sealed, which protects the TENG from the influence of environment. As for the reason of output enhancement under water, it is inferred that the water can act as back electrode of the silicone rubber.

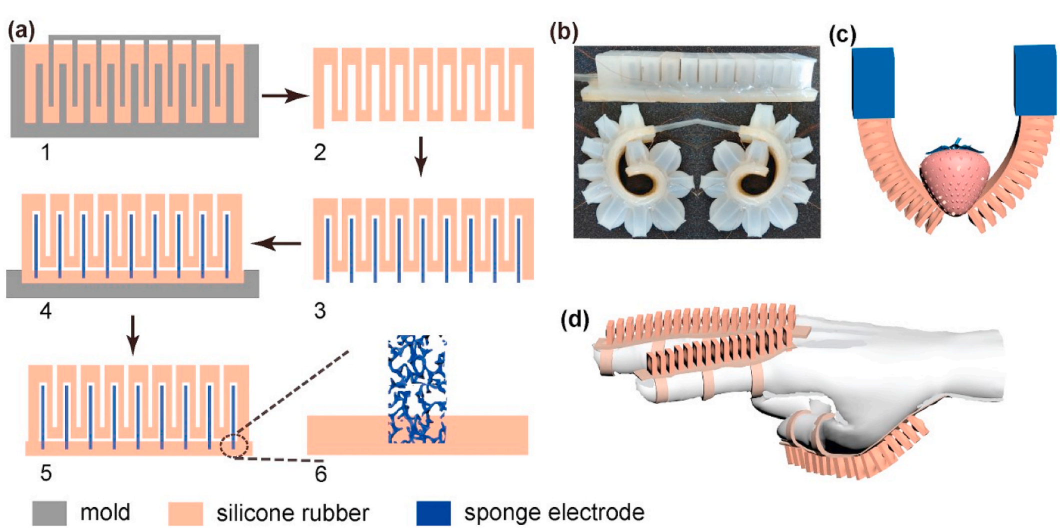

Fig. 1. Scheme illustration of the sensorized pneumatic soft robot (PSA). (a) Fabrication processes of the sensorized PSA. (b) Photographs of the fabricated sensorized PSA. Applications of the sensorized PSAs in (c) soft gripper and (d) assisting glove.

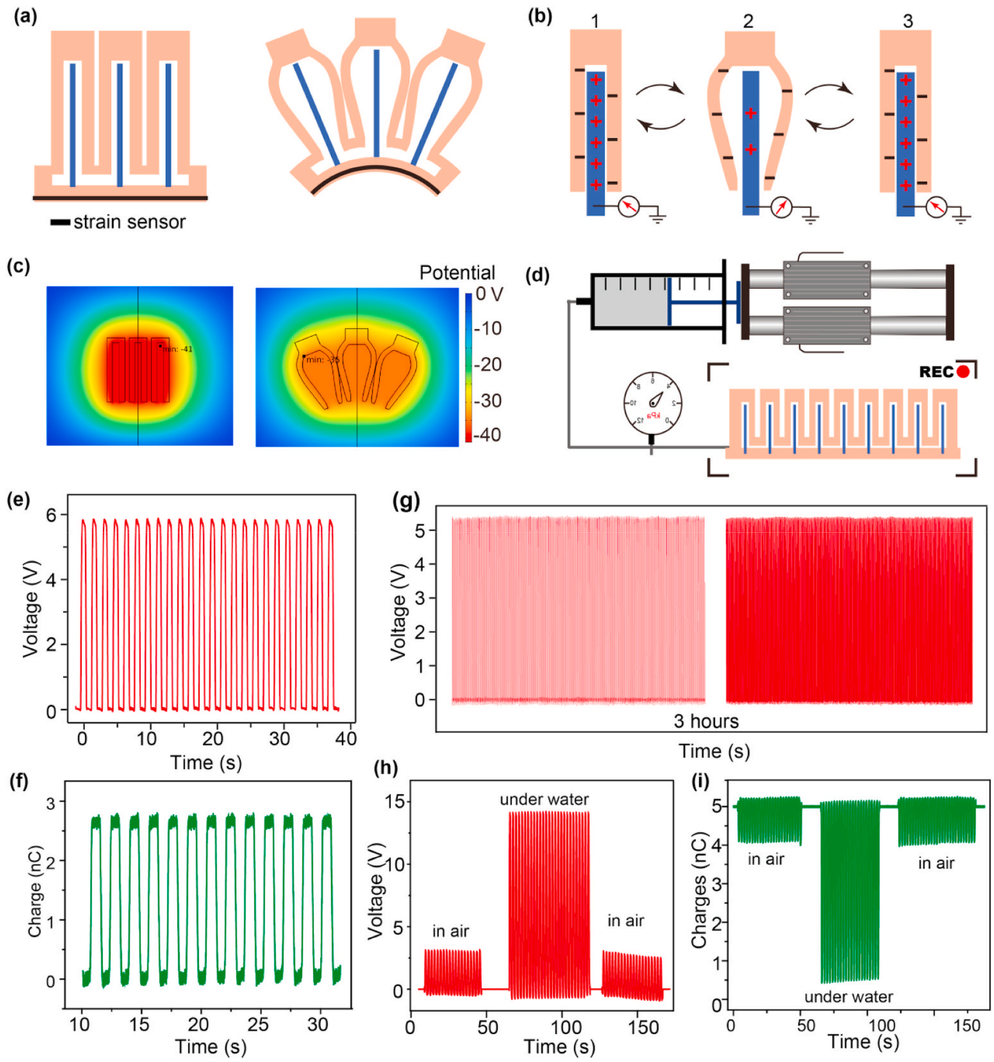

Fig. 2. Principle and basic outputs of the TENG. (a) Comparison of the traditional strain sensor and TENG-based self-powered sensor. (b) Working mechanism of the TENG under short-circuit condition. (c) Simulation of the electric potential distribution of the TENG under open-circuit condition. (d) Diagram of the experimental system including the apparatus of the gas pump, pressure meter and PSA. (e) Open-circuit voltage and (f) transferred charges of the TENG. (g) Open-circuit voltage of a TENG tested for 3 h. (h) Open-circuit voltage and (i) transferred charges of a TENG under dry and wet conditions.

The TENG was not single-electrode but contact-separation mode.

The sensor performance regarding to the pose of PSA's tip was investigated as well. In order to minimize the influence of gravity force and friction force, the PSA was placed sideway and floated on the water. When inflating, the PSA freely bend into a perfect arc with a constant curvature. The bending angle of the PSA was measured from the pictures recorded by a digital camera. Besides, the pressure inside the chambers and the electrical outputs were measured in real time. Controlled by a linear motor, the gas was pumped into the PSA. The gas volume increased step by step from 2/3 mL to 26/3 mL by 2/3 mL each time. As a result, the pressure inside the chambers increased from 0.25 kPa to 13 kPa with the slop of 1.59 kPa/mL (The red line in Fig. 3a). The angles between the tangents at both ends of the PSA are displayed in Fig. 3a with blue color, which could be fitted by a straight line, showing the pneumatic process of the PSA has good linearity. The voltage of TENG versus gas volume are plotted in Fig. 3b. As the gas volume increased from 2/3 mL to 26/3 mL, the voltage of TENG increased from 3 V to 44 V. The linear fitting slop between voltage and volume is 5.05 V/mL. Moreover, the transferred charges also increased from 1 nC to 16.5 nC. The relation between bending angle and voltage was derived and plotted in Fig. 3c. As the bending angle increased from 29° to 290°, the voltage linearly increased from 3 V to 44 V with a fitted slop of 0.17 V/°. The voltage of TENG sensor has good linearity and sensitivity regard to the bending angle of PSA. Based on the constant curvature model, the position and orientation of the PSA's tip can be derived from the bending angle and the length of the PSA. Therefore, the sensorized PSA has possessed the proprioception to feel its own shape.

However, the PSA is so soft that prone to be affected by external forces. Experiments were carried out to investigate the sensor performance when the PSA was hung up under gravity. The gas was pumped into the PSA with the gas volume increment of 10/3 mL each time. The corresponding voltage output is plotted in Fig. 3d. The voltage increased step by step as the PSA bending stepwisely. The voltage at the static state was very stable and the dynamic response was very quick. After 5 steps, the PSA bended at an angle of 300° and the voltage reached 24 V. At a reversed process, the gas was pumped out and the PSA unbend step by step. The voltage backtracked to original value with high repeatability. The poses of the PSA were recorded by a camera to measure the angle between the tangents at both ends. Fig. 3e shows two pictures when the PSA was bended after 4 and 5 steps respectively. The corresponding angles were 200° and 300°. The voltage and bending angle can be well fitted by a straight line with a slop of 0.076 V/° (Fig. 3f). Because of the influence of gravity, the shape of the PSA was not a perfect arc as in water but more like a helix.

The sensorized PSA was demonstrated as a universal gripper to catch objects with different sizes or weights and give feedback information. As illustrated in Fig. 4a, two sensorized PSA were fixed at an acrylic frame face to face with 150 mm gap. The bending of the PSA fingers narrowed the gap and gripped the objects. When the sizes of the objects are different, the bending angles and the voltage outputs are different.

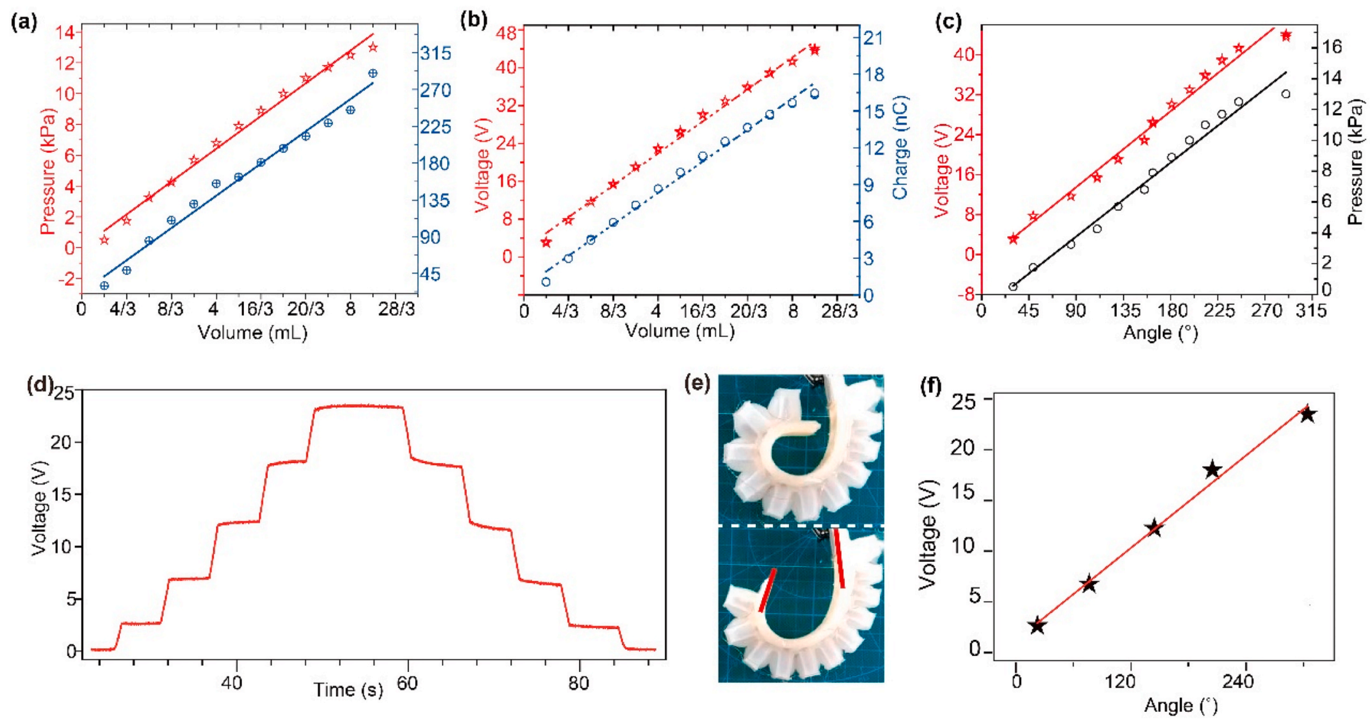

Fig. 3. Investigation of the sensor performance when TENGs were connected in parallel. (a) The pneumatic performance of the PSA. The pressure and bending angle were linearly related to the gas volume. (b) The open-circuit voltage and transferred charge of the TENGs under different gas volumes. (c) The open-circuit voltage and gas pressure versus bending angle. (d) The open-circuit voltage when the PSA under stepwise bending. (e) The photographs of the PSA under different bending angle. (f) The linear fitting of the voltage versus the bend angle.

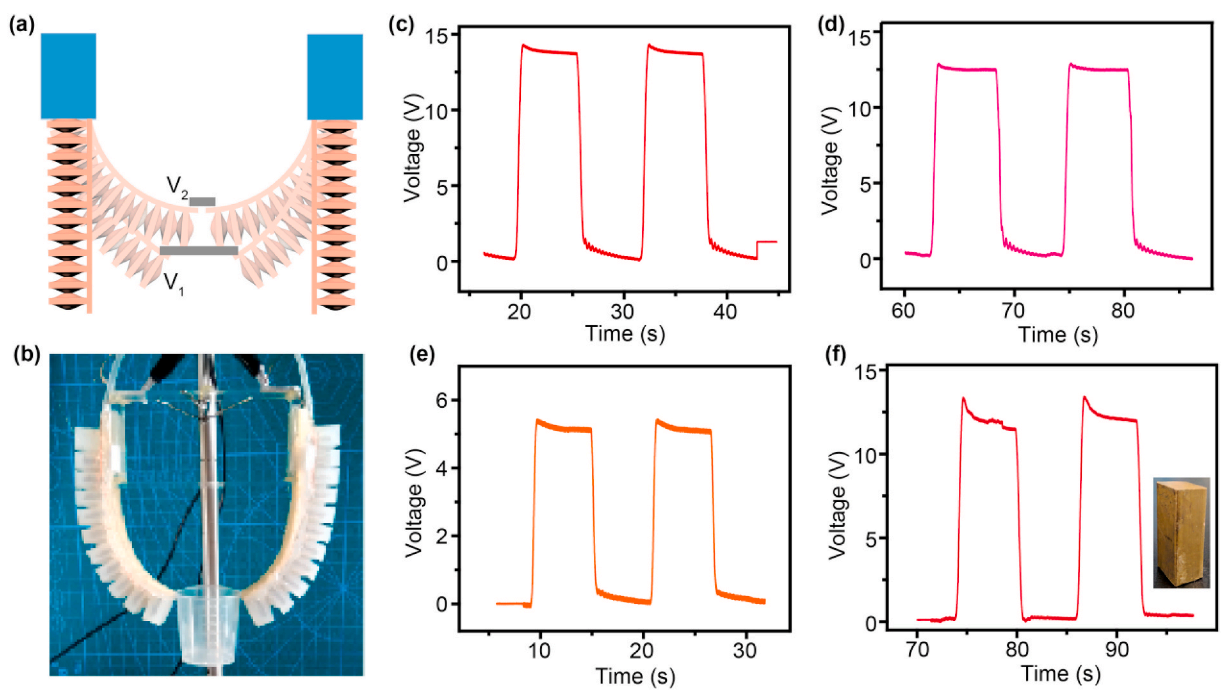

Fig. 4. Demonstration of the sensorized PSA in a soft gripper. (a) Schematic illustration of the soft gripper that assembled from two sensorized PSA. (b) Photograph of the gripper catched a small cup. The open-circuit voltage when catching (c) a small cup and (d) a middle size cup. The open-circuit voltage when catching (e) a large cup and (f) a 36g copper block added into.

Fig. 4b shows the picture of a sensorized universal gripper when it caught a small cup (30 mm in diameter). The bending angle of the PSA was about 65° and the corresponding voltage output is shown in Fig. 4c. At the grasping process, the voltage increased simultaneously, and reached 14 V when firmly caught the cup. When the cup was dropped, the voltage decreased every quickly to about 2 V and then generally to the original value with oscillatory attenuation. The decay process of the voltage was well accorded to the attenuation motion of the PSA, showing a high sensitivity. When it caught a middle cup (85 mm in diameter), the output voltage was only 12 V (Fig. 4d). And the voltage dropped to 5 V when it caught a large cup (135 mm in diameter), as illustrated in Fig. 4e. The voltage decreased because that smaller bending angle was needed for catching a larger one. Moreover, when the gripper caught the large cup that contained a 36 g metal block, the voltage increased to about 11 V (Fig. 4f). This is because catching a heaver object needs larger pressure. These experimental results showed that the sensorized PSA-based gripper can catch different objects and evaluate the size or weight in real-time.

However, in most situations, the PSA usually do not bend into a perfect arc because the influence of external forces. Fig. 3f shows a PSA curled up into helical because of the gravity, which complicates the configuration sensing. It needs a serial of sensors to detect the curvatures at different parts of the PSA, and help rebuild the shape based on the piecewise constant curvature model (Fig. 5a) [37,38]. The challenge lies in how the segments and sensors are arranged. If the segments are too small, it is inaccuracy. If too large, it needs a lot of sensors and will consume too much energy. The optimal scheme is that segments are divided according to the chambers, whose expansion cause the bending. The sensorized PSA here is conformed to the optimal scheme that every chamber contains a TENG to serve as the local bending angle sensor independently. In this way, the PSA was divided into 10 segments by the chambers. And the bending angle of each segment was reflected by the TENG inside the chamber.

The relation between the bending angle of a chamber and the voltage of the corresponding TENG was tested. Only the middle one chamber of the PSA was left to bend freely, while the others were wrapped with the tape to limit its bending. The PSA was also placed sideways and floated on water to eliminate the influence of the external forces. The gas volume, gas pressure, voltage output and bending angle of that chamber were recorded and shown in Fig. 5b. As the gas volume increased from 4/3 mL to 6 mL, the pressure raised from 2 kPa to 12 kPa. The pressured gas caused the expanding of the chamber, which folded the PSA in the middle with the angle ranged from 8° to 60°. The output voltage increased from 4 V to 10.8 V, and had a good linear relation to the gas volume with the fitting slope of 1.43 V/mL. The relation between the voltage and bending angle was derived and plotted in Fig. 5c, which could be fitted by a straight line with the slope of 0.1147°/V. These experiments were repeated for multiple times and the data were highly overlapped. It indicated that the TENG sensor performance is stable and repeatable, showing the potential of self-powered sensor for local bending angle of the PSA.

To verify the distributed sensing performance, the voltage outputs of the TENGs were recorded independently to monitor the shape of the PSA under different conditions. Firstly, the whole PSA was floated on the water sideways so that every chamber was able to bend freely by pressured gas. The voltage of all 10 TENGs were exhibited one by one in Fig. 5d. The average voltage was about 9 V with small fluctuation of about ±1 V, which reflected the bending angle of each chamber was very

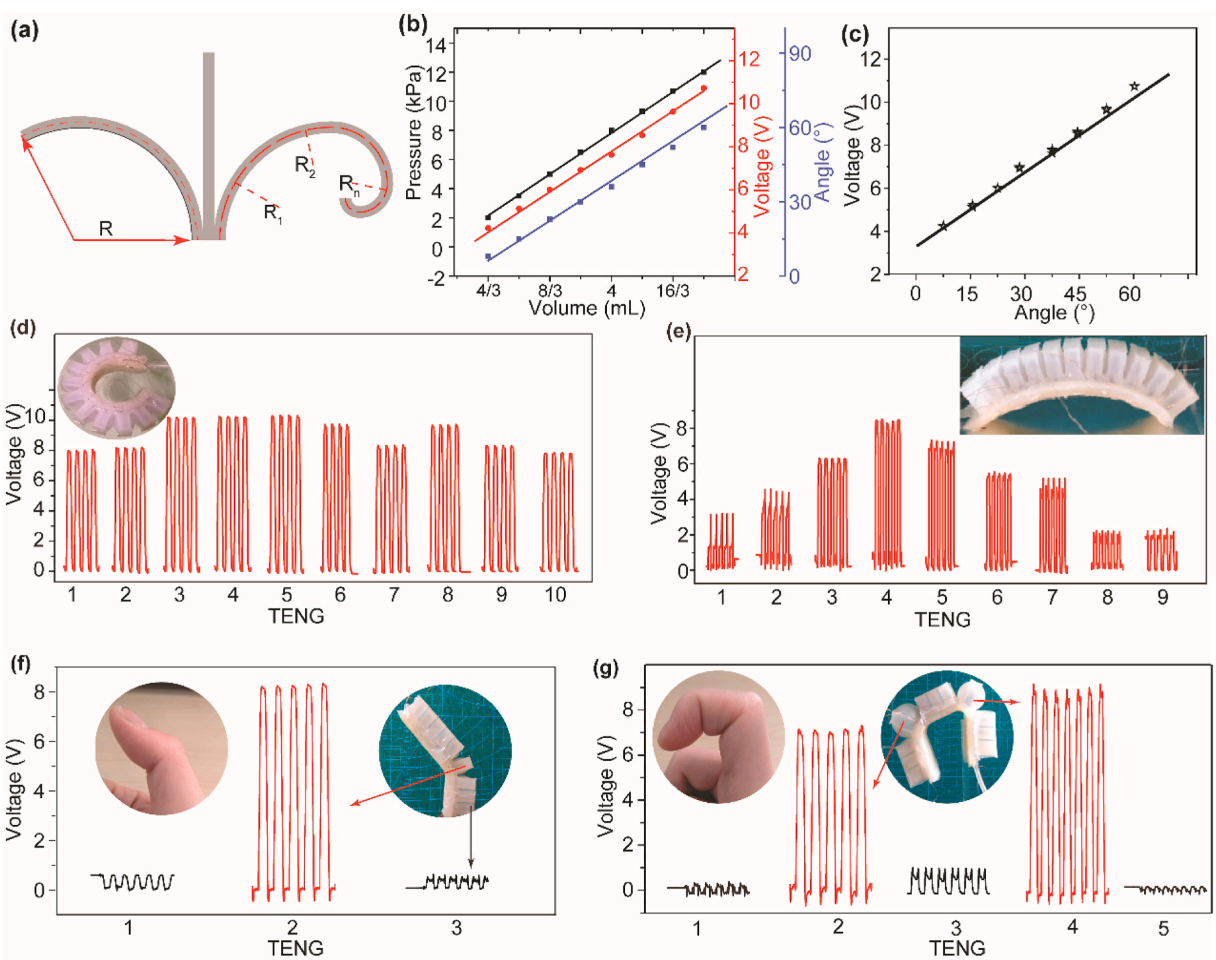

Fig. 5. Investigation of the distributed sensors for piecewise PSA. (a) Comparison of the constant curvature model and multi-segment piecewise constant curvature model. (b) The gas pressure, local bending angle and open-circuit voltage of a chamber versus the gas volume. (c) The relation between the open-circuit voltage of a chamber and the local bending angle. (d) The open-circuit voltage of each TENG when the PSA bended freely on water. (e) The open-circuit voltage of each TENG when the PSA was placed flatwise on a table. (f) The average voltage of the joint and links of the PSA when it was mechanically programmed into thumb shape. (h) The average voltage of the joints and links of the PSA when it was programmed into index finger shape.

close. As shown in the inserted picture of Fig. 5d, the whole PSA body bended into an arc with an approximate constant curvature, which agreed with the voltage. Then, the PSA was placed flatwise on the table. Under pressure, the PSA bended upward and arched on the table. The two ends of the PSA stood on the table to support the weight, which restricted the expanding and bending of the nearby chambers. Near the middle position, the force is smaller, and the bending angle is larger. The picture of the arched PSA is inserted in Fig. 5e, and the voltage of each chamber is also displayed. The voltage outputs near the two ends were smaller than that near the middle segments, which is in line with the shape of the PSA. These results indicated that the distributed self-powered TENG sensors are able to perceive the piecewise curvature of the PSA, which is significant for the modeling and controlling of the compliant PSA.

Furthermore, the PSAs were mechanical programmed into different segments to intimate fingers, whose gestures were detected by the TENG sensors. The PSA was divided into three segments to imitating the thumb. Part 1 and 3 contained five chambers respectively and were wrapped by tape to prevent it bending, while part 2 contained only one chamber and was free to bend. The photographs of a thumb and the programmed 3 segmented PSA are shown in Fig. 5f. The voltages of the three parts were recorded when the PSA bending. The average voltage output of each TENG in part 1 and 3 were merely about 0.5 V, because the bending was limited. The voltage of part 2 was about 8 V, corresponding to the bending angle of 44° at the joint. In addition, the PSA was reprogrammed into 5 segments to imitate an index finger. Part 1, 3 and 5 contained three chambers respectively and were wrapped by tape to prevent their bending. Part 2 and 4 had one chamber each and were free to bend like the finger joints, as illustrated in the inserted photographs of Fig. 5g. The average voltage of each chamber in part 1, 3 and 5 were 0.5 V, 1 V and 0.5 V respectively, while part 2 and 4 were 7 V and 9 V. The output voltage of different parts could reflect the gesture of SPA finger very well, indicating the potential application in wearable devices and robotic hands.

The segmented finger-like PSA shows potential applications in humanoid fingers and assisting glove, as depicted in Fig. 6a. The demonstration was performed on a wooden humanoid-hand. The 3 segmented PSA was fixed on the thumb and the 5 segmented one was fixed on the index finger. The PSA guided the fingers to bend while the sensors gave feedback on the gesture. As shown in Fig. 6b, the voltage output at the thumb joint was about 9 V when it bended to 51°. But the voltage dropped to about 5 V when the bending angle was smaller, about 39° (Fig. 6c). The two joints of the index finger were driven by the 5 segmented PSA to bend simultaneously. The voltage at the first joint was above 10 V (Fig. 6d), which is slightly larger than the voltage of the second joint shown in Fig. 6e. It is expected that the sensorized PSA can be used as assisting glove to help disabled person make gesture and handle different objects.

3. Conclusion

In conclusion, a sensorized PSA was developed by integrating TENGs into the chambers to serve as the proprioception sensors of configuration. Connected in parallel, the total voltage output of the TENGs was linearly related to the total bending angle of the PSA. Independently, the 10 TENGs served as distributed sensors to detect the bending angle of every segments of the piecewise PSA. Hence, the sensorized PSA could perceive its own shape, which was tested under different conditions. As a demonstration, the sensorized PSA were assembled into a universal soft gripper and humanoid fingers respectively. With the proprioception, they are smarter and safer when interacting with environments or humankind.

CRediT authorship contribution statement

Jian Chen: Conceptualization, Methodology, Visualization, Data curation, Writing - original draft. **Kai Han:** Conceptualization, Methodology, Validation, Resources, Writing - review & editing. **Jianjun**

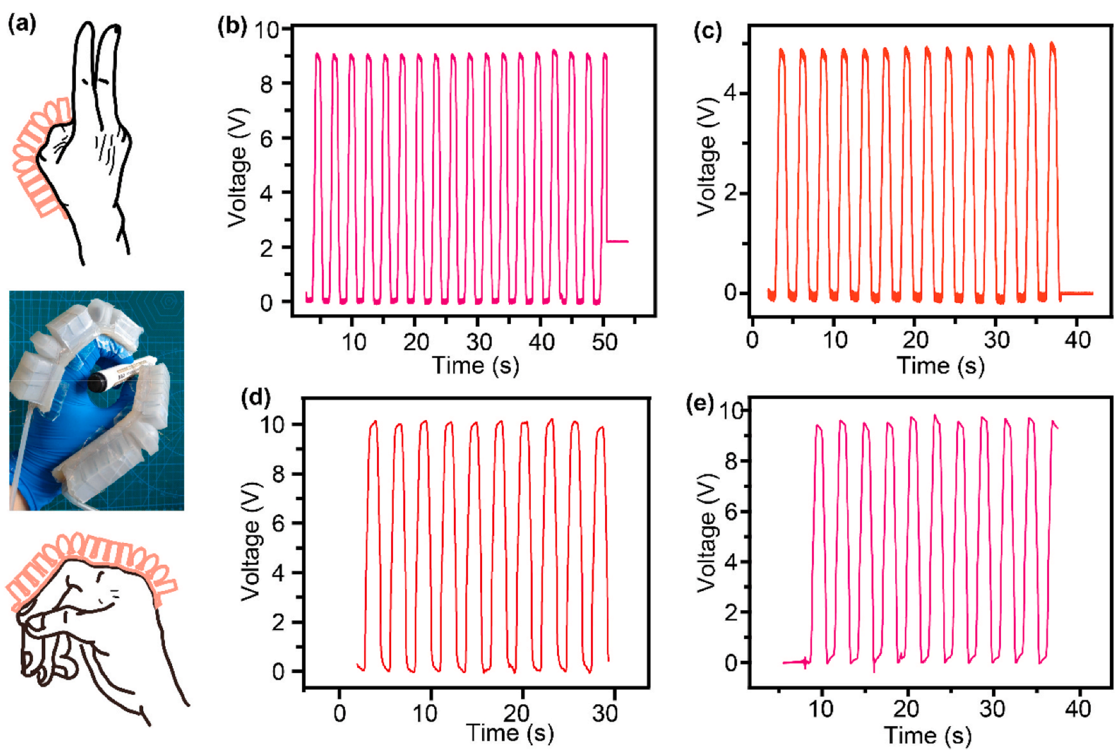

Fig. 6. Demonstration of the sensorized PSA in assisting glove. (a) Schematic illustration of the sensorized PSA fixed on fingers. (b) and (c) The open-circuit voltage of the thumb joint when bending at different angles. The open-circuit voltage of (d) the first joint and (e) the second joint of the index finger shape PSA when bending.

Luo: Resources, Writing - review & editing. **Liang Xu:** Methodology, Resources, Formal analysis. **Wei Tang:** Methodology, Supervision, Writing - review & editing. **Zhong Lin Wang:** Methodology, Supervision, Writing - review & editing.

Declaration of competing interest

The authors declare that they have no known competing financial interests or personal relationships that could have appeared to influence the work reported in this paper.

Acknowledgments

The research was supported by the National Key R & D Project from the Minister of Science and Technology (2016YFA0202704), Youth Innovation Promotion Association, CAS, Beijing Municipal Science and Technology Commission (Z171100000317001, Z171100002017017, Y3993113DF), and National Natural Science Foundation of China (Grant No. 51605033, 51432005, 5151101243, 51561145021).

References

[1] R.F. Shepherd, F. Ilievski, W. Choi, S.A. Morin, A.A. Stokes, A.D. Mazzeo, X. Chen, M. Wang, G.M. Whitesides, Proc. Natl. Acad. Sci. U. S. A. 108 (2011) 20400–20403.
[2] S. Terryn, J. Brancart, D. Lefeber, G. Van Assche, B. Vanderborght, Sci. Robot. 2 (2017).
[3] S. Coyle, C. Majidi, P. LeDuc, K.J. Hsia, Extreme Mech. Lett. 22 (2018) 51–59.
[4] E.W. Hawkes, L.H. Blumenschein, J.D. Greer, A.M. Okamura, Sci. Robot. 2 (2017).
[5] F. Schmitt, O. Piccin, L. Barbé, B. Bayle, Front. Roboti. AI 5 (2018).
[6] C. Walsh, Nat. Rev. Mater. 3 (2018) 78–80.
[7] H. Banerjee, Z.T.H. Tse, H. Ren, Int. J. Robot Autom. 33 (2018).
[8] H. Wang, M. Totaro, L. Beccai, Adv. Sci. (Weinh) 5 (2018) 1800541.
[9] M. Luo, E.H. Skorina, W. Tao, F. Chen, S. Ozel, Y. Sun, C.D. Onal, Soft Robot. 4 (2017) 117–125.
[10] Y. Li, Y. Chen, Y. Li, in: IEEE Robotics and Automation Letters 4, 2019, pp. 1402–1408.
[11] Soft Robotics: Trends, Applications and Challenges, 2017.
[12] B.S. Homberg, R.K. Katzschmann, M.R. Dogar, D. Rus, Aut. Robots 43 (2018) 681–696.
[13] J. Wirekoh, L. Valle, N. Pol, Y.L. Park, Soft Robot. 6 (2019) 768–777.
[14] H.A. Wurdemann, S. Sareh, A. Shafti, Y. Noh, A. Faragasso, D.S. Chathuranga, L. Hongbin, S. Hirai, K. Althoefer, Conf. Proc. IEEE Eng. Med. Biol. Soc. (2015) 8026–8029, 2015.
[15] S. Ozel, N.A. Keskin, D. Khea, C.D. Onal, Sensor Actuator Phys. 236 (2015) 349–356.
[16] S. Sareh, Y. Noh, M. Li, T. Ranzani, H. Liu, K. Althoefer, Smart Mater. Struct. 24 (2015).
[17] Z.L. Wang, Nano Energy 68 (2020).
[18] J. Chen, H. Guo, Z. Wu, G. Xu, Y. Zi, C. Hu, Z.L. Wang, Nano Energy 64 (2019).
[19] S. Lin, L. Xu, A. Chi Wang, Z.L. Wang, Nat. Commun. 11 (2020) 399.
[20] C. Zhang, J. Chen, W. Xuan, S. Huang, B. You, W. Li, L. Sun, H. Jin, X. Wang, S. Dong, J. Luo, A.J. Flewitt, Z.L. Wang, Nat. Commun. 11 (2020) 58.
[21] H. Qin, G. Gu, W. Shang, H. Luo, W. Zhang, P. Cui, B. Zhang, J. Guo, G. Cheng, Z. Du, Nano Energy 68 (2020).
[22] H. Qin, G. Cheng, Y. Zi, G. Gu, B. Zhang, W. Shang, F. Yang, J. Yang, Z. Du, Z. L. Wang, Adv. Funct. Mater. 28 (2018).
[23] H. Guo, X. Pu, J. Chen, Y. Meng, M.-H. Yeh, G. Liu, Q. Tang, B. Chen, D. Liu, S. Qi, C. Wu, C. Hu, J. Wang, Z.L. Wang, Sci. Robot. 3 (2018).
[24] T. Bu, T. Xiao, Z. Yang, G. Liu, X. Fu, J. Nie, T. Guo, Y. Pang, J. Zhao, F. Xi, C. Zhang, Z.L. Wang, Adv. Mater. 30 (2018), e1800066.
[25] Y. Zou, P. Tan, B. Shi, H. Ouyang, D. Jiang, Z. Liu, H. Li, M. Yu, C. Wang, X. Qu, L. Zhao, Y. Fan, Z.L. Wang, Z. Li, Nat. Commun. 10 (2019) 2695.
[26] M.S. Rasel, P. Maharjan, M. Salauddin, M.T. Rahman, H.O. Cho, J.W. Kim, J. Y. Park, Nano Energy 49 (2018) 603–613.
[27] G.-Z. Yang, J. Bellingham, P.E. Dupont, P. Fischer, L. Floridi, R. Full, N. Jacobstein, V. Kumar, M. McNutt, R. Merrifield, B.J. Nelson, B. Scassellati, M. Taddeo, R. Taylor, M. Veloso, Z.L. Wang, R. Wood, Sci. Robot. 3 (2018).
[28] C. Lu, J. Chen, T. Jiang, G. Gu, W. Tang, Z.L. Wang, Adv. Mater. Technol. 3 (2018).
[29] K. Zhao, G. Gu, Y. Zhang, B. Zhang, F. Yang, L. Zhao, M. Zheng, G. Cheng, Z. Du, Nano Energy 53 (2018) 898–905.
[30] Y.C. Lai, J. Deng, R. Liu, Y.C. Hsiao, S.L. Zhang, W. Peng, H.M. Wu, X. Wang, Z. L. Wang, Adv. Mater. 30 (2018), e1801114.
[31] A. Ahmed, S.L. Zhang, I. Hassan, Z. Saadatnia, Y. Zi, J. Zu, Z.L. Wang, Extreme Mech. Lett. 13 (2017) 25–35.
[32] X. Chen, T. Jiang, Y. Yao, L. Xu, Z. Zhao, Z.L. Wang, Adv. Funct. Mater. 26 (2016) 4906–4913.
[33] T. Chen, Q. Shi, M. Zhu, T. He, L. Sun, L. Yang, C. Lee, ACS Nano 12 (2018) 11561–11571.
[34] S. Liu, Y. Li, W. Guo, X. Huang, L. Xu, Y.-C. Lai, C. Zhang, H. Wu, Nano Energy 65 (2019).
[35] L. Li, T. Wang, T. Jin, P. Ma, Y. Jiang, G. Yuan, Y. Tian, in: 2019 IEEE International Conference on Robotics and Biomimetics (ROBIO), 2019, pp. 211–216.
[36] J. Chen, B. Chen, K. Han, W. Tang, Z.L. Wang, Adv. Mater. Technol. 4 (2019).
[37] R.K. Katzschmann, C.D. Santina, Y. Toshimitsu, A. Bicchi, D. Rus, in: 2019 2nd IEEE International Conference on Soft Robotics (RoboSoft), 2019, pp. 454–461.
[38] G. Runge, M. Wiese, L. Gunther, A. Raatz, in: 2017 3rd International Conference on Control, Automation and Robotics (ICCAR), 2017, pp. 7–14.

Dr. Jian Chen received his B.S. degree in Central South University in 2014, and his Ph.D. degree in Condensed Matter Physics from University of Chinese Academy of Sciences in 2019. He is now a postdoctoral fellow in Nanyang Technological University. His research interests include triboelectric nanogenerators, self-powered systems and soft robot.

Mr. Kai Han received his B.E. degree in Macromolecular Materials and Engineering from Qingdao University in 2012, and his M.E. degree in Applied Chemistry from Shanghai University in 2015. He is now a Ph.D. student in Beijing Institute of Nanoenergy and Nanosystems, Chinese Academy of Sciences, under the supervision of Prof. Zhong Lin Wang. His research interests include triboelectric nanogenerators, self-powered electrochemistry and systems.

Dr. Jianjun Luo received his B.S. degree in Applied Chemistry from Jinan University in 2013, and his Ph.D. degree in Condensed Matter Physics from University of Chinese Academy of Sciences in 2018. He is now a postdoctoral fellow in Beijing Institute of Nanoenergy and Nanosystems, Chinese Academy of Sciences, under the supervision of Prof. Zhong Lin Wang. His research interests include triboelectric nanogenerators, self-powered systems and supercapacitors.

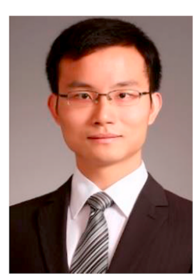

Dr. Liang Xu received his Ph.D. degree from Tsinghua University (THU) in 2012, with awards of Excellent Doctoral Dissertation of THU and Excellent Graduate of Beijing. Before that he achieved bachelor's degree of mechanical engineering in Huazhong University of Science & Technology (HUST) in 2007. He is now an associate professor in Beijing Institute of Nanoenergy and Nanosystems, Chinese Academy of Sciences (CAS), under the supervision of Prof. Zhong Lin Wang. His research interests include nanogenerators and self-powered nanosystems, fundamental tribological phenomena, scanning probe microscopy and molecular dynamics simulation.

Dr. Wei Tang is a professor in Beijing Institute of Nanoenergy and Nanosystems, Chinese Academy of Sciences. He received his B.S. and Ph.D. degree from School of Physics and School of Electronics Engineering and Computer Science, in 2008 and 2013, respectively, from Peking University, China. After graduation, he worked in Beijing Institute of Nanoenergy and Nanosystems as a postdoc research fellow. His research interests include Micro/Nano engineering, triboelectric nanogenerator, self-powered micro/nano system and wireless sensing network.

Prof. Zhong Lin Wang received his Ph.D. from Arizona State University in physics. He now is the Hightower Chair in Materials Science and Engineering, Regents' Professor, Engineering Distinguished Professor and Director, Center for Nanostructure Characterization, at Georgia Tech. Prof. Wang has made original and innovative contributions to the synthesis, discovery, characterization and understanding of fundamental physical properties of oxide nanobelts and nanowires, as well as applications of nanowires in energy sciences, electronics, optoelectronics and biological science. His discovery and breakthroughs in developing nanogenerators established the principle and technological roadmap for harvesting mechanical energy from the environment and biological systems for powering personal electronics. His research on self-powered nanosystems has inspired the worldwide effort in academia and industry for studying energy for micro-nano-systems, which is now a distinct disciplinary in energy research and future sensor networks. He coined and pioneered the field of piezotronics and piezophototronics by introducing piezoelectric potential gated charge transport process in fabricating new electronic and optoelectronic devices. Details can be found at: www.nanoscience.gatech.edu.